Multiplexed High-Throughput Image Cytometry Using Encoded Carriers

Ilya Ravkin*, Vladimir Temov, Aaron Nelson, Michael Zarowitz, Matthew Hoopes, Yuli Verhovsky, Gregory Ascue, Simon Goldbard, Oren Beske, Bhagyashree Bhagwat, Holly Marciniak
Vitra Bioscience, 2450 Bayshore Parkway, Mountain View, California, 94043

ABSTRACT

Image cytometry has made possible the collection and analysis of multiparameter cellular information. The wider use of image cytometry in drug screening will depend on its throughput, efficiency, repeatability, and on the added benefits compared with less sophisticated but faster methods. Throughput (number of datapoints per unit of time) and efficiency (number of datapoints from the given amount of reagents or plate area) are addressed here by screening multiple cell lines simultaneously using encoded carriers (CellCards®). CellCards are rectangular particles with an expandable color barcode and a transparent section for cellular readout. Before performing the assay, each cell line is grown on a different class of carriers. CellCards, with attached cells, are mixed and dispensed into a microtiter plate where the assay is performed. Next the plates are imaged, decoded and the cells associated with each CellCard class are analyzed. Using CellCards the efficiency is increased by the multiplexing factor (the number of cell lines analyzed in each well). We routinely run assays with a multiplex factor of ten. Throughput is additionally addressed by working at the lowest possible magnification for a given assay. Decoding of CellCards requires one image per well in 96-well microtiter plate format. The system provides the added benefit of internal consistency since the data can be normalized to controls within each well.

Keywords: multiplexed cell analysis, multiparameter imaging and measurement, algorithms for cell analysis, encoded carriers, high-throughput cytometry

1. INTRODUCTION

Many new technologies seek to increase both information density and the quality of data gathered from experiments. Microarray technologies, both positional and non-positional[1,2,4,5], have provided an efficient way to do this. Furthermore, by combining microarray technologies with microtiter plates one can multiplex experiments within a single well, thus increasing information density and simultaneously obtaining data on multiple analytes[3,5]. This approach also provides an increase in data quality and robustness derived from the ability to include internal controls and to correlate data obtained from identical reaction conditions[5]. Although this type of approach is routinely used in analyzing DNA or proteins, it has never been successfully applied to the study of cells. We present here a new non-positional array technology that for the first time enables this type of analysis to be done with a diverse set of cellular assays.

The CellCard system shows remarkable flexibility in that it can be used with a large range of assays from very fast assays like nuclear translocation and reporter gene assays, to long incubation assays such as apoptosis and cytotoxicity. To illustrate the platform's utility and compatibility with a diverse set of cellular assays we described in this paper its use in two different assays. By combining multiple cell types in the same well across a variety of assays this technology can provide a unique insight into the profiling of compounds by simultaneously obtaining potency, selectivity, and mechanistic information on each tested compound.

2. ENCODED CARRIERS

The CellCard particles are the basis of the cellular multiplexing platform presented here. These particles have embedded in them a positional code that is optically readable. In addition, they can support the growth of cells and are usable for

* iravkin@vitrabio.com

optical imaging of cells. The configuration of CellCards depends on the desired number of classes (codes), on the preferred manufacturing methods, on the detection modalities of both the code and the cells, and on the format of the system (e.g., slides, microtiter plates of given density, etc.).

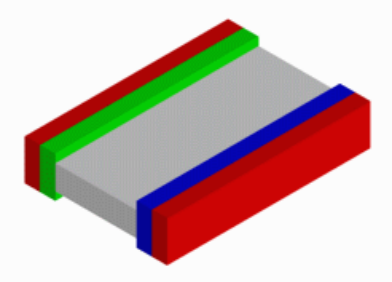

Fig. 1. CellCard with two coding bands on each side and a recessed clear cell readout area in the middle.

The current design separates the area of the particle that is used for encoding from that used for biological readout. The latter is the useful area and the former is the overhead of encoding. Since the code within each particle is positional, it can use as few as two distinguishable states (e.g., colors). The number of coding positions (e.g., bands) is then chosen to encode the required number of classes.

Fig.1 shows a CellCard in conceptual form. The particles have an aspect ratio that causes them naturally to lie flat. Since in practice a CellCard may lie either side up, the number of distinguishable codes is given by the following formula:

$N_D = (N_T - N_S)/2 + N_S$, Where N_D is the number of distinguishable codes, N_T is the total number of codes, N_S is the number of symmetrical codes. For more reliable recognition we impose an additional restriction that adjacent bands can not be of the same color. With this: $N_T = (M(M-1))^2$, $N_S = M(M-1)$, where M is the number of colors. Thus, if three colors are used for the coding bands, $N_D = 21$. This number of distinguishable classes is sufficient for cellular multiplexing in 96-well microtiter plates.

The carriers have overall dimensions of L=500µm, W=350µm, H=100µm. The recess of the middle area provides better cell retention during dispensing and diffusion of reagents during the assay phase. The carriers are made of biocompatible materials and demonstrate no cellular toxicity.

3. PROCEDURE FOR PERFORMING ASSAYS ON CELLCARDS IN MICROPLATES

3.1. Overview

The diagram in Fig. 2 illustrates the steps of performing an assay on CellCard carriers. 1) The carriers are dispersed in 6-well plates, the cells are plated onto of the carriers and incubated overnight to allow cells to attach and spread; 2) the carriers with attached cells are combined and mixed; 3) approximately 100 carriers are dispensed from the mixing tube into each well of a microtiter plate; 4) the carriers are dispersed to minimize overlaps; 5) the

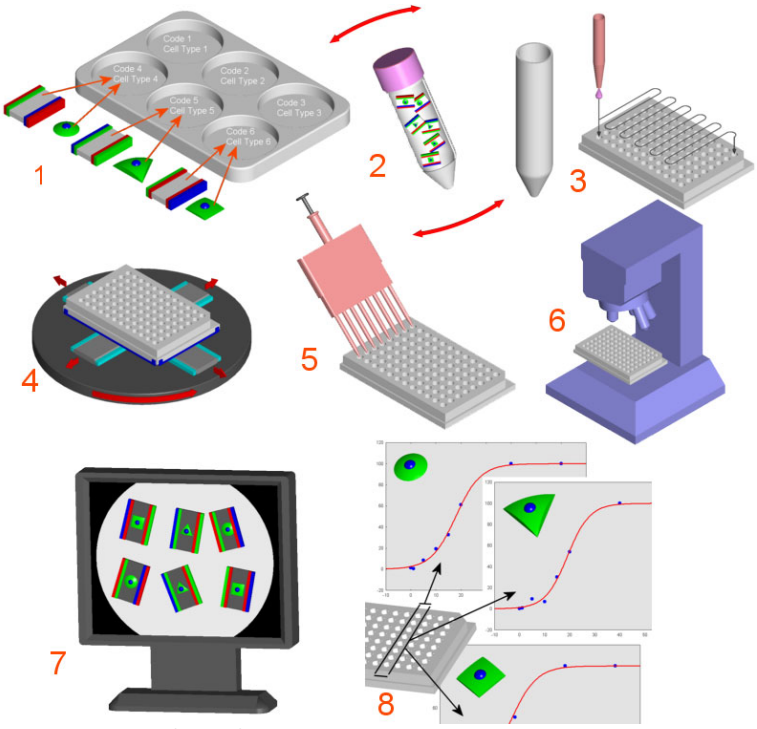

Fig. 2. Procedure for performing assays on CellCard carriers: 1-plating cells on carriers, 2-mixing, 3-dispensing, 4-dispersing, 5-performing the assay, 6-image acquisition, 7-image analysis for decoding and cell measurements, 8-data analysis.

assay is performed as usual; 6 - images of each well are acquired in both brightfield and fluorescence mode; 7) images are analyzed to decode the carriers and make assay-specific measurements; 8) numerical well-level data is analyzed and plotted.

3.2. Dispensing

The transfer of a homogeneous mixture of CellCard particles carrying multiple cell lines to an assay plate is an essential step in the screening process using the CellCard system. It requires minimizing shear forces that might detach cells while maintaining the hydrodynamic and surface tension forces that are used to transfer the CellCards from the dispensing container to the microtiter wells. The CellCard dispenser (Vitra Bioscience, Mountain View, CA) is based on a syringe-driven liquid handling system. Custom tips and accurate liquid control ensure proper transfer of the particles.

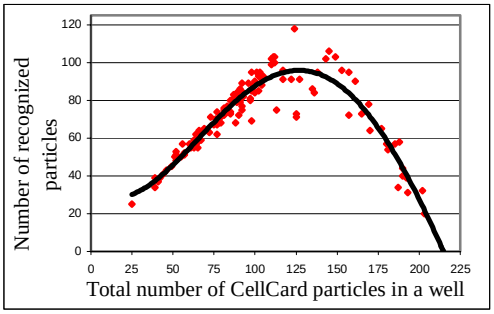

Fig. 3. Number of recognized CellCard particles as a function of the total number of particles in a well.

The CellCard dispenser is optimized to enable recognition by the software of the largest number of carriers. Too many carriers would cause overlaps and reduce recognition. Fig. 3 shows that the maximal number of recognized CellCards in a 7-mm well is around 100 and it can be achieved with around 110 dispensed CellCards (the counts were produced after dispersing, see below).

3.3. Dispersing

The goal of dispersing is to provide a single layer of CellCards in order to minimize overlap, and thereby maximize the number that can be recognized by the software. Although the particles are small, their density is more than twice that of the solution in which they are dispensed, so they sink rapidly to the bottom. Once in the wells, the particles rest in a random clustering as seen in Fig. 5 (left). The CellCard disperser (Vitra Bioscience, Mountain View, CA) uses two orthogonal bearings mounted to an orbital shaker (DS-500 from VWR, West Chester, PA) to convert the orbital motion of the shaker to the linear motion required for dispersion. Speed, distance of travel, and the amount of liquid in the well have been optimized for best dispersion. Linear as opposed to circular motion is essential as it prevents formation of a vortex, which would move the particles to the center of the well, defeating the purpose of dispersing. An example of CellCards before and after dispersion is shown in Fig. 5.

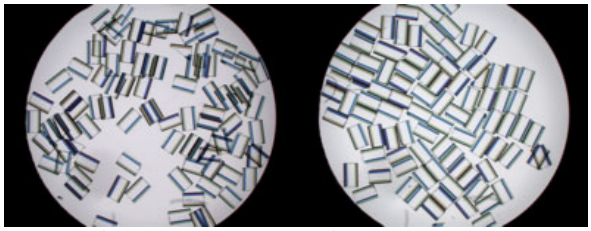
Fig. 5. Left - Carriers in a well before dispersing, Right - same well after dispersing

4. IMAGING OF CELLCARDS

Imaging of CellCard carriers poses some specific challenges caused by the thickness of the particles and by the need to image the whole well. To this end, we have developed the CellCard Analyzer (Vitra Bioscience, Mountain View, CA), to enable brightfield illumination (for decoding), focusing, and fluorescence imaging of whole wells with CellCards that have cells both “face up” and “face down”.

4.1. Brightfield illumination

Shadow-free illumination of carriers in the whole well is created in the system by a custom integrating sphere with 24 color LEDs. This configuration provides sufficient light intensity to achieve integration times from 1 to 3ms. Switching time is < 1ms. The light from the LEDs is reflected from the diffuse white interior of the integrating sphere, thus illuminating the top of the sphere uniformly. This area of the sphere provides illumination to the well that is uniform

from all angles, as well as uniform throughout the field of view. This is the ideal illumination condition for brightfield microscopy, and is optimal for reading the code bands.

4.2. Focusing on CellCards

Imaging-based autofocus algorithms historically have been very limited in performance due to less than ideal fluorescent targets. Because they are imaged in brightfield, CellCards provide an ideal target, high in both brightness and contrast. With less than 1 ms integration time for brightfield images performance is now limited only by hardware speed. The algorithm used is an extension of the focusing algorithm described previously ([8]). A Z-seek is started in a heuristically determined direction and speed. A contrast function is calculated for each image during the seek process. After a sufficient number of images has been collected the Z-seek is halted and the Z axis is moved to the position corresponding to the interpolated maximum of contrast. Autofocusing on CellCards with a 2X 0.10 NA objective typically takes about 1 second and is reproducible to 1µ accuracy.

A unique characteristic of autofocusing on CellCards using a small depth of field objective is the bimodal contrast curve shown in Fig. 7. CellCards have two points of maximum contrast corresponding to their two sides. A 2X 0.10 NA Plan Apochromat objective has a depth of field of about 120µm, larger than the thickness of the particles, so the contrast curve has only one peak (Fig. 8). A 10X 0.30 NA Plan Fluor objective used for imaging of individual carriers has depth of field of 10µm - short enough to generate two maxima. This allows focusing on both surfaces in only one pass in brightfield, which makes it fast. Switching to fluorescence, the images from both surfaces can be captured and the one that contains the cells in focus retained. The CellCard reader implements the following imaging strategy: it first autofocuses and gathers images looking at the whole well with a 2X objective. If required by the particular assay, the well is then sub-scanned using a higher magnification objective. Known focal offsets are applied between objective changes, so the autofocus seek for higher magnification objectives is needed only to accommodate imperfections in the microtiter plate. The seek range is narrow, so each sub-field is autofocused very quickly.

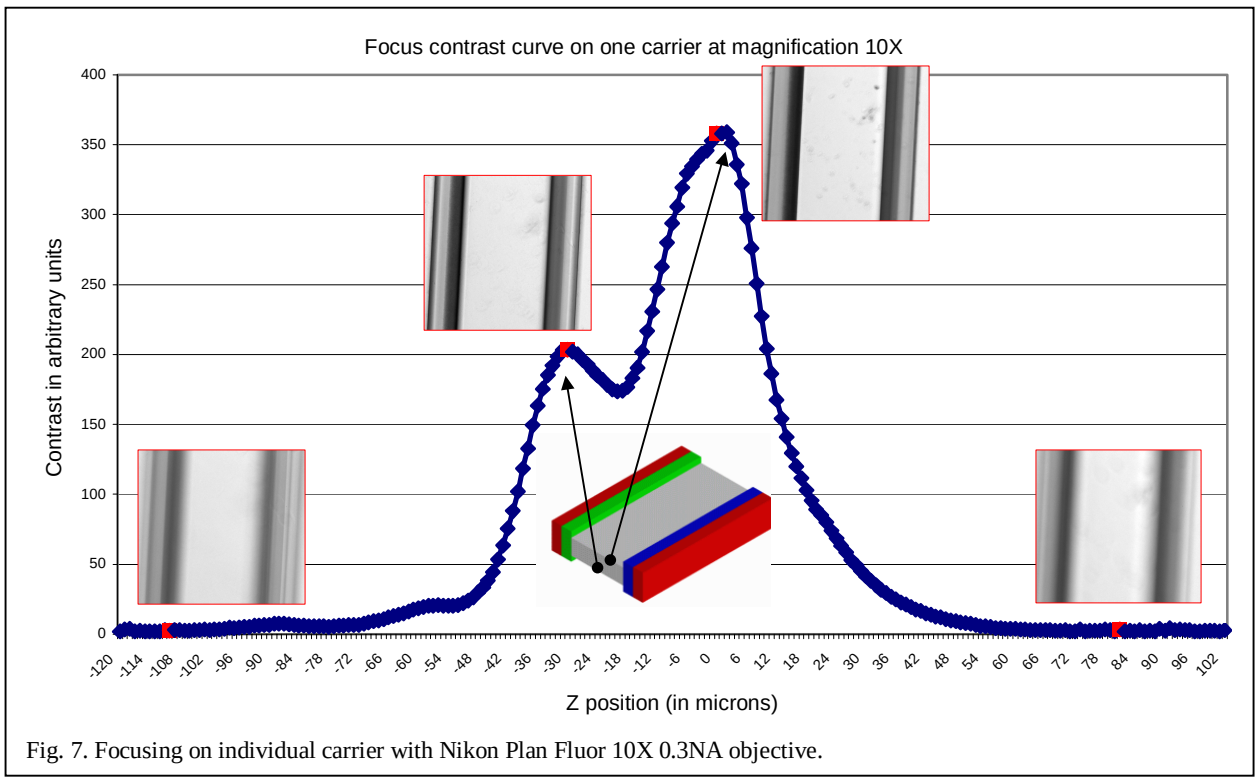

Fig. 7. Focusing on individual carrier with Nikon Plan Fluor 10X 0.3NA objective.

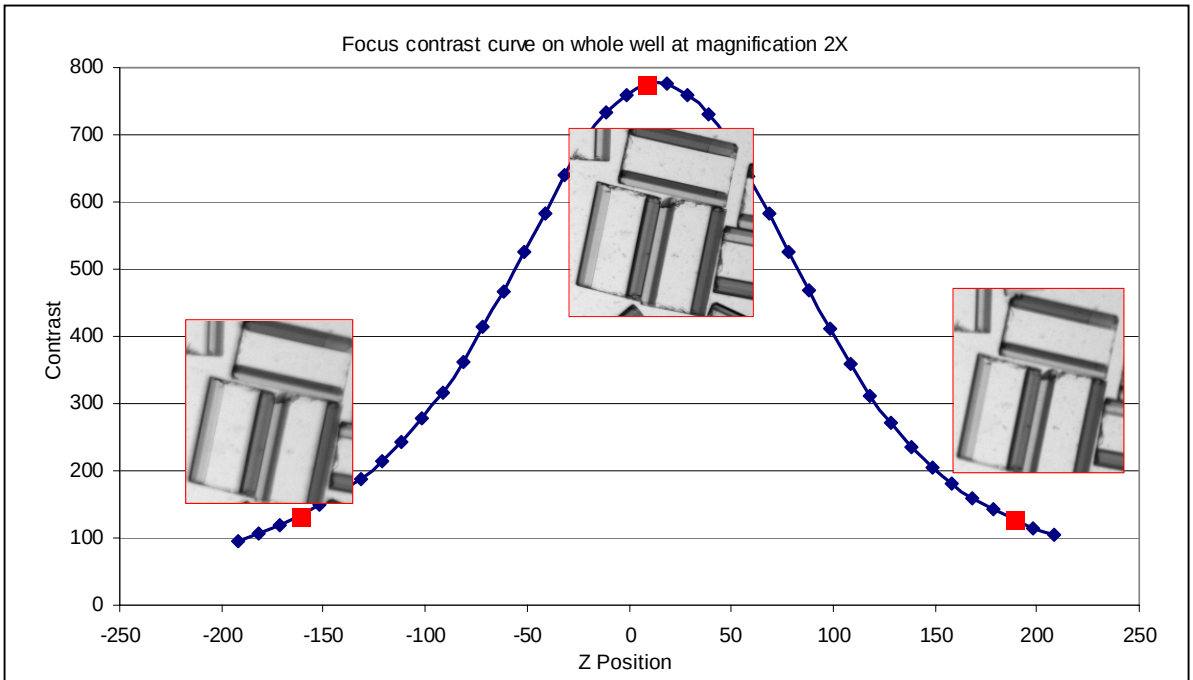

Fig. 8. Focusing on whole well with Nikon Plan Apochromat 2X 0.1NA objective.

4.3. Fluorescence imaging of cells on CellCards

When cells are initially grown on CellCards (before dispensing them in the 96 well plate) they are all on the top surface of the particles. However, after mixing and dispensing the carriers can land with the cells in either orientation: up or down. This has implications for the staining and subsequent imaging of the cells. The current design of the carriers (Fig. 1) has a recessed area to achieve good diffusion of reagents under the carrier to the cells on its bottom surface. The carriers are made of a material

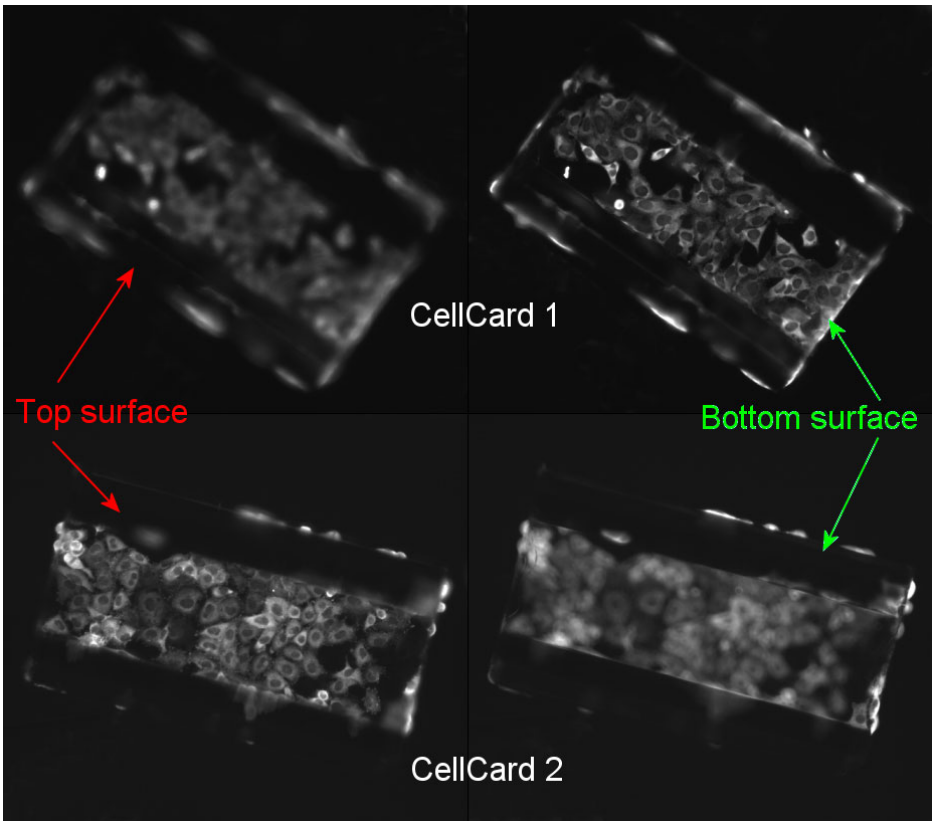

Fig. 9. Two carriers imaged at top and bottom surfaces with a Nikon Plan Fluor 10X 0.3NA objective.

that does not introduce optical distortions; the middle section is clear with parallel surfaces and the thickness of 30-50μm, which is 3-5 times thinner than a coverslip. Compared with the thickness of the bottom of a microtiter plate (0.7 mm for the 96-well Viewplate, Packard Biosciences; Boston, MA, used here) the added thickness is not significant. However, the particles add two more interface surfaces. Fig. 9 shows two carriers in the same well imaged at top and bottom surfaces. Our experience shows that there is no image degradation when imaging through the carrier at objective magnifications from 2X to 20X. We also did not observe any consistent or significant difference in the intensities of images from the top and bottom surfaces of the carriers.

5. RECOGNITION AND DECODING OF CELLCARDS

The ability to recognize and decode CellCards is at the core of this platform. The first step in the decoding process is background equalization. The image of the background is produced by morphological closing of the acquired RGB image of the whole well (Fig. 13, left) with a structuring element that completely removes the carriers. The original image is then divided by this image at every pixel in each color plane.

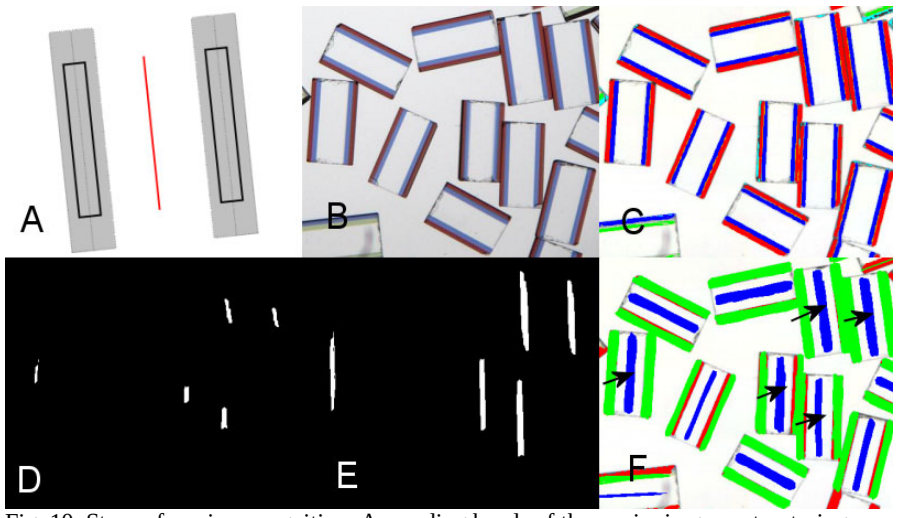

Fig. 10. Steps of carrier recognition. A – coding bands of the carrier in gray, structuring element for erosion in black and structuring element for dilation in red shown at one of the orientations, B – fragment of a well image before background equalization, C – color masks, D – erosion of band mask by structuring element of A produces carrier markers, E – dilation of carrier markers of D by structuring element of A produces medial lines of carriers, F – carriers with coding bands and medial lines produced after pattern matching at all orientations where carriers of orientation shown in A, D and E are indicated by arrows.

The RGB image with equalized background is then converted to hue, saturation, value (HSV) color space. For each of the colors used in the coding bands of the carriers a color mask is produced by AND-ing double-sided threshold masks for hue, saturation and value. All of these masks are OR-ed into the band mask, which is used for detection of carriers.

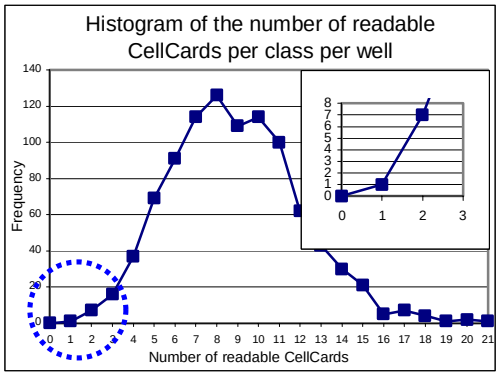

Fig. 12. A typical histogram of the number of readable CellCards per cell type per well (for 10 classes in each well). The inset shows in larger scale that there are no wells with 0 carriers and one well with 1 carrier per cell type. This data point may be removed as unreliable.

Cellcards appear in the image as a disjoint pair of double color bands at random orientations. The model of a carrier image is shown in gray in Fig 10 A. The detection of carriers is based on erosion of the band image by the structuring element shown in black in Fig 10 A. This structuring element is a pair of rectangles of a length that is smaller than the shortest CellCard and a width that is about half the width of the coding band. The result of such erosion – carrier markers - is shown in Fig. 10 D. The marker image is dilated by the structuring element shown in Fig. 10 A in red giving medial lines of carriers (Fig 10 E). This

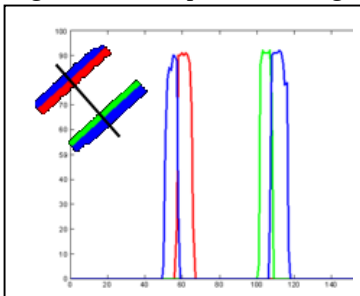

Fig. 11. Color bands and their projections. Code BR-GB

process is repeated for the orientations of the structuring element from 0° to 180° with 4° step. The medial lines from all orientations are accumulated and shown together with band masks in Fig. 10 F.

After all CellCards are detected, those that are too short, broken or are overlapping other CellCards are rejected. The algorithm has the option of retaining the non-overlapping portions of overlapping CellCards, which is useful for some assays. Since the CellCard image is at this stage a disjoint set of two coding bands there is a chance that a space between two CellCards may be misidentified as a CellCard. To prevent this, a check is performed to ensure that each coding band belongs to only one CellCard.

When the location and orientation of each CellCard is known, the algorithm calculates the projection (number of pixels) of each of the color masks on the direction perpendicular to the medial axis of a CellCard. These projections are shown in Fig.11. The sequence of color peaks in the plot gives the code. In addition, the measurement mask is produced for each CellCard. Results are represented visually to the user in the format shown in Fig. 13. A representative distribution of the numbers of CellCards in a well for each of the 10 classes is shown in Fig. 12. The CellCard recognition software as well as cell analysis software described below is implemented using Matlab (MathWorks, Natick, MA) and its Image Processing Toolbox.

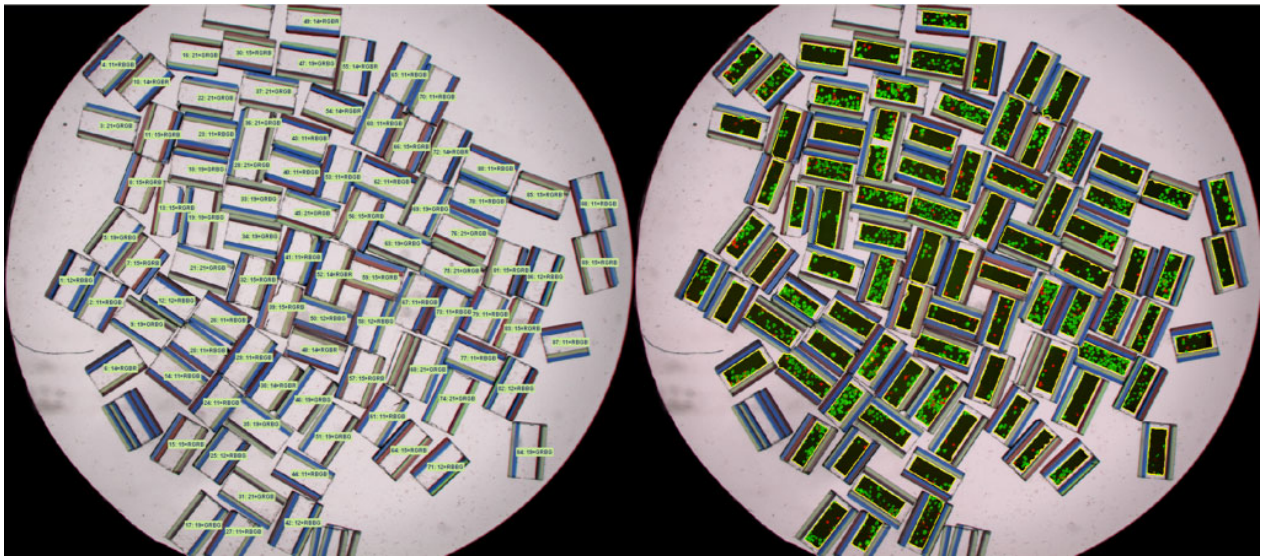

Fig. 13 Left - Recognized carriers with class assignment, Right - measurement areas with composite fluorescence images and overlaid contours inscribed into each carrier. Note that overlapping carriers and those partially in the image are neither recognized nor used for cell measurements.

6. ANALYSIS OF CELL IMAGES ON CELLCARDS

The analysis of brightfield images described above provides the means of deconvolving the mixture of cell types residing on different CellCard classes. The cellular measures, however, are derived from images of cells, which are typically fluorescent. We have imaged on CellCards cells with intrinsic fluorescence (e.g., GFP), cells stained with fluorescence-conjugated antibodies, cells stained with colorimetric dyes, and even unstained cells. Here we will concentrate on the analysis of fluorescent cell images. As described above, the CellCard platform is based on utilizing and analyzing all available well area. Thus, the desire is to work at the lowest possible magnification in order to attain the greatest throughput. The lowest possible magnification is determined by the demands of cell image analysis and depends on the assay. In this paper we give examples of 3 assays with different image resolution requirements: counting of nuclei (for cell proliferation/cytotoxicity measures), nuclear translocation and receptor internalization.

In cellular imaging assays, the measure (or measures) used to characterize the assay is far removed from the signal registered by the camera. Different algorithms will produce different assay measures on the same image. This is especially acute for redistribution assays (e.g., nuclear translocation) where the total intensity may not change and the

assay result may depend more on the algorithm than on the raw image. In order to decide which resolution is minimally acceptable for a given assay and algorithm we analyze the same well area at different optical magnifications or/and the same set of images at different interpolated magnifications. In a similar manner, the effect of the cell number is analyzed by comparing measures from images of different size. To compare results we use quality functions discussed in the next paragraph. This analysis is done on cells grown directly in plates, not on carriers, to make the results easier to compare with that of other researchers.

6.1 Assay and algorithm quality measures for cell-imaging assays

In high throughput drug screening it is common to evaluate the quality of assays by a statistical parameter that depends on the dynamic range and variability of the assay. Several such parameters have been introduced with z-value[7] being the most popular. Z-value is given by the following formula:

$Z = 1 - 3(\frac{SD_{pos} + SD_{neg}}{|M_{pos} - M_{neg}|})$, where SD is standard deviation, M is mean, *pos* and *neg* are the two extreme states of the assay, which define its dynamic range. Z value ranges from $-\infty$ to 1. For cell-based assays, z-values above 0.5 are considered good. This measures proved to be very useful to capture and compare variability caused by assay biology and by instrumentation (e.g., pipetting). Cell assays based on imaging introduce several new variables: imaging resolution, size of the imaged area and the data extraction algorithm. Size of the imaged area is a variable because usually less than the whole well is imaged and analyzed. Having a quality measure, like the z-value, allows us to optimize variables that are under our control, e.g., find the best data extraction algorithm. Here we will deal with specific cell image analysis algorithms and will use the quality measure to optimize image resolution and size.

In addition to introducing new variables, cellular imaging assays may lead us to reconsider the quality measure itself. An assay measure derived from an image may be computationally very complex. It may contain operations that have the effect of saturating the values from the positive and negative states of the assay, thus artificially reducing variability. This may happen unintentionally and even without being realized. Moreover, if the values of the assay for its positive and negative states do not overlap (and if they do it may not be a very useful assay), the z-value can be manipulated intentionally, by applying a mathematical transformation that maps all positive values into a single value and all negative values into another single value. One way of dealing with this is the use in the quality measure of a dose-dependent sequence of assay states (dose-curve) with doses being close enough to each other, so that artificial manipulation would be impossible. This leads to the following measure, which we refer to as the "v-value":

$V = 1 - 6(\frac{SD_{of_fit}}{|M_{pos} - M_{neg}|})$, where $SD_{of_fit} = \sqrt{\sum_{1}^{n} \frac{(f_{\exp} - f_{\mathrm{mod}})^2}{n}}$, $f_{\exp}$ and f_{mod} are experimental and model values of the assay measure at a given concentration, n is the number of experimental points in the dose curve.
The v-value reverts to z-value if there are only two dose points. The model may be chosen depending on the nature of response, with logistic curves often being the natural choice. Alternatively, as is the case with the two examples given below, no specific model is used and the average of several replicas is used as f_{mod} in the above equation.

The v-value is less susceptible to saturation artifacts caused by computation than z-value. There is also another subtle difference. Standard deviation in the middle of the dose-response curve is often larger than the standard deviation at the extremes. This is because the maximal point on the curve is often determined at saturating concentration, and so any dispensing error has little effect on the response; the minimal point is usually zero concentration and it also avoids dispensing errors. In contrast, the effect of volume errors has its maximal effect in the middle of the dose-response curve. Taking the whole curve into account gives a more realistic measure of the assay data quality.

6.3 Nuclear translocation assay

Intracellular imaging makes possible the analysis of the movement of molecular targets inside the cell. Many transcription factors and kinases translocate from cytoplasm to nucleus in the course of the activation process. We have developed a method of analysis of images of translocation events based on a model of joint distribution of counter- and

signal stains. For algorithm development we used a series of 12 images of translocation of the transcription factor NFκB in MCF7 cells in response to TNFα concentration (Fig. 18). To find a robust measure of nuclear translocation we have defined a model of spatial distribution of the nuclear counterstain and of the signal stain as it moves from the cytoplasm to the nucleus. The model was studied under some perturbations in order to find measures that are robust.

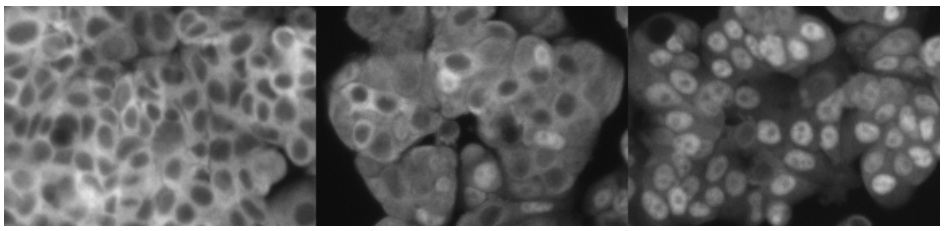

Fig. 18. Nuclear translocation assay of NFkB in MCF7 cells. Left-negative, middle-intermediate, right-positive states. Images of FITC stain acquired with a 10X objective.

The model of cell staining comprises a bell-shaped intensity distribution of counterstain, which is shown in blue, and a bell-shaped distribution of signal stain, which is shown in green in Fig. 19. For the negative case the distribution of signal stain is wider and has a bell-shaped crater. Profiles through the real cells (Fig. 19, right) show substantial similarity to the model profiles. (Profile C is plotted through two cell, profile D – through three cells. All profiles are independently normalized to their intensity maxima.).

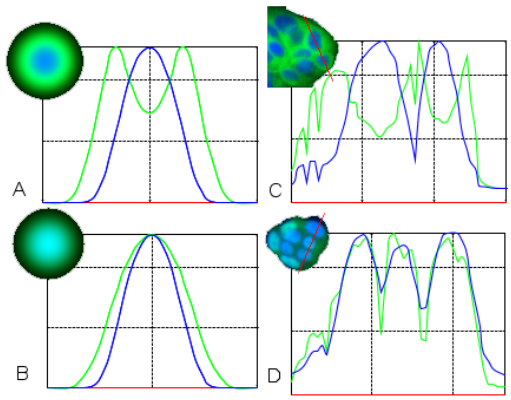

Fig. 19. Images and profiles through model and real cells. A,B – model; C,D – real, A,C – negative, B,D – positive. Blue – counterstain, green – signal stain.

In analyzing nuclear translocation images, the natural approach is to segment the image into nuclei and cytoplasm of individual cells, measure the amount of signal stain in each and calculate a measure of translocation as the difference or the ratio of the two[17,18]. A variation on this approach is to analyze signal stain in smaller compartments defined by their spatial relation to the center or the boundary of the nucleus[19,20]. In all cases these methods require image segmentation. Our goal was to develop a method that would not require, or at least would not critically depend on segmentation, because segmentation methods do not scale well with magnification.

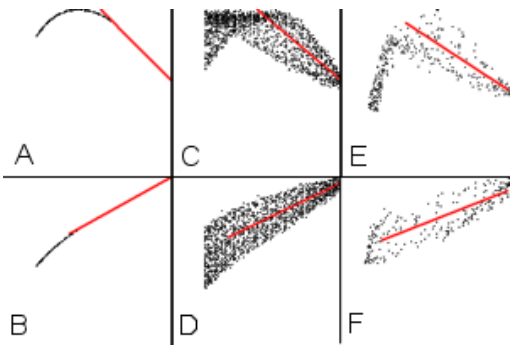

Fig. 20. Cross-histograms of counterstain (X) and signal stain (Y) in ideal model (A,B), perturbed model (C,D) and a real cell (E,F). Scale on both axes is 0-255. Red lines show the calculated approximation.

To derive stable measures that characterize transitions from the negative to the positive case, we analyzed joint distributions of the stains on the model and on real cells; see Fig. 20. In the ideal case, the model spatial stain distributions are circularly symmetrical and aligned, as shown in Fig. 19 (A,B). The cross-histogram for this case is shown in Fig. 20 (A,B). If the model is perturbed by offsetting the centers of the two stains, by changing shape from circular to oval, or by adding noise, the distributions become fuzzy as shown in Fig. 20 (C,D). Typical

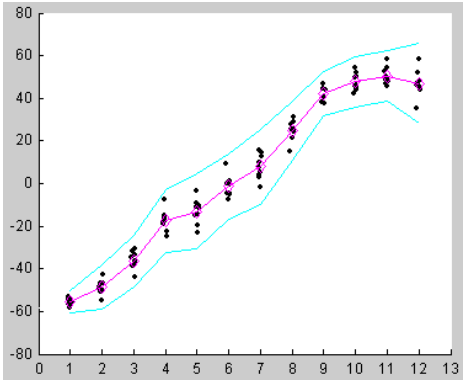

Fig. 22. Nuclear translocation dose curve. X-TNFα concentration. Y- average cell slope. V-value=0.74

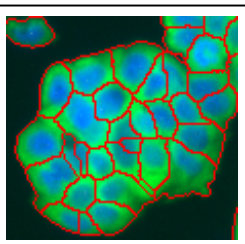

Fig. 21. Cells separated by watershed lines.

negative and positive real cells have cross-histogram as shown in Fig 20 (E,F). These distributions suggest that a translocation measure can be defined as the slope of a straight-line segment approximating the right side of the cross-histogram. This portion of the distribution corresponds to the more intense nuclear staining and is also close to the center of the nucleus. The farther from the center, the more diffuse the distribution, and the less reliable the approximation become. The portion of the distribution that is used for approximation with the straight line is found by plotting the approximated slope going from right to left and selecting the range where this approximation is the most stable.

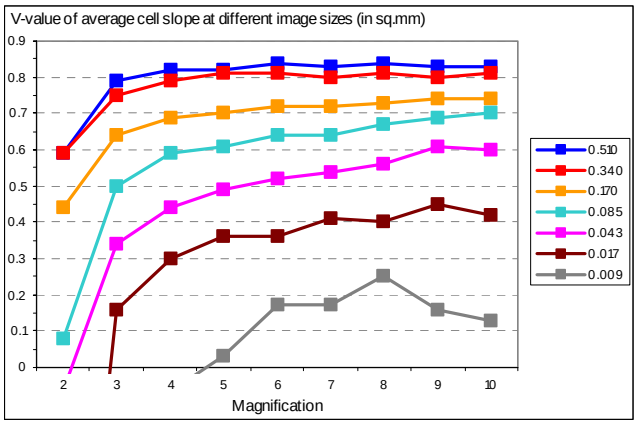

Fig. 23. V-value for nuclear translocation measure as a function of interpolated magnification at different image sizes.

The described method can be applied globally to the whole image, to an individual cell, or to a cluster of cells. To apply it to individual cells, there is no need to know the cell or nuclear boundary. All that is needed, is to know the area within which a separate cell is contained. To find these areas we used watershed[10,11] of the inverted image of the counterstain. Fig. 21 shows separation lines found by this method. The parameter used to characterize a population of cells, e.g., an image, or a well, is the average value of the individual cell slope. This parameter was evaluated in a dose-dependent set of images (Fig. 18); the resulting curve is shown in Fig. 22.

The behavior of this algorithm was studied as a function of interpolated image magnification – from the original 10X down to 2X, and image size. The v-value concept introduced above was used a measure of quality. Image interpolation was done by the bilinear method. To study image-size dependency the original image at each point in the curve was divided into fragment images of smaller sizes. Each of the smaller images was used to produce the translocation measure and these measures were used in the formula for v-value. The results in Fig. 23 show that the algorithm reaches a plateau of v-value around 0.8 at magnifications of 4X or greater and image sizes of 0.34 mm^2 or greater.

The algorithm described above has several desirable features; it does not require segmentation into cellular compartments; it scales well with magnification; it has no user-settable parameters; it is not sensitive to overall image intensity, or to variation in intensity among cells; it is based on a model that allows us to test the effects of disturbances (e.g., noise, irregular shape) and find a stable measure; it can be used on the individual cell level or globally.

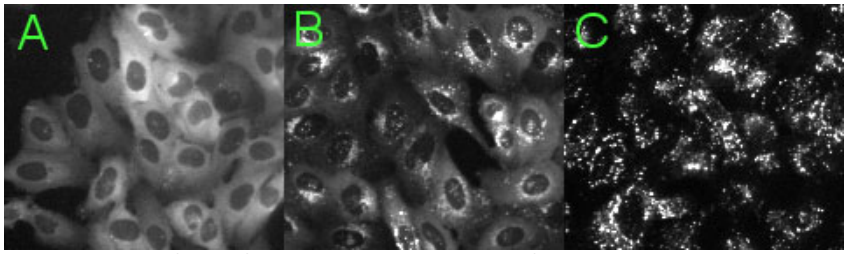

Fig. 24. Images of Transfluor assay at objective magnification 10X with 2*2 binning: A – negative, B – intermediate, C – positive.

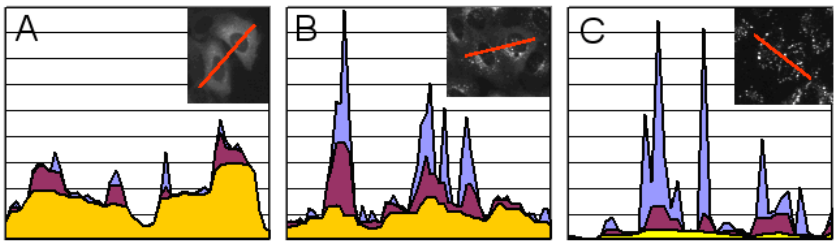

Fig. 25. Brightness profiles through cells in the original image (blue), in the image opened by structuring element of size 1 (red) and in the image opened by structuring element of size 4 (yellow). Left - negative, middle - intermediate and right - positive states of Transfluor assay.

6.4 Receptor internalization (Transfluor) assay

The Transfluor assay (commercialized by Norak Bioscience) is used to measure activity of G-protein coupled receptors (GPCR). This assay

employs green fluorescen protein (GFP) fused to β-arrestin as its readout. The basis of the assay is to measure the sub-cellular localization of this fusion protein, which changes depending on receptor activity. Since β-arrestin is involved in the regulation of many GPCR's it is thought of as a general assay. That is, one assay can serve to measure activity from different classes of GPCRs.

Examples of Transfluor images are shown in Fig. 24. Receptor internalization in the Transfluor assay causes images to change from diffuse staining to more granular staining. We have developed a method for analyzing Transfluor images, which formalizes the intuitive notion of granularity in a simple measure. The basis of the method is the concept known in mathematical morphology as size distribution[9], granulometry[14], pattern spectrum[13] or granular spectrum[16]. This distribution is produced by a series of openings of the original image with structuring elements of increasing size. At each step the volume of the open image is calculated as the sum of all pixels. Fig. 25 shows how openings of increasing size affect images with different granularity. The difference in volume at the successive steps of opening is the granular spectrum, given by the formula:

$$G(n) = V(\gamma_{n-1}(X)) - V(\gamma_n(X))$$

Where X is the image, n is the opening size, also referred to as thickness, $G(n)$ is the granular spectrum at n-th opening, $\gamma_n(X)$ is n-th opening of image X, $V(X)$ is the volume (sum of pixels values) of image X. Granular spectra for the negative, intermediate and positive states of the assay are shown in Fig. 26 To characterize the different states of the assay we introduced a measure called relative granularity, given by the following formula:

$$RG = G(T1)/G(T2),$$

Where RG is relative granularity, $T1$ is the thickness most characteristic of the granular (positive) state of the assay, $T2$ is the thickness most characteristic of the diffuse (negative) state of the assay. $T1$ and $T2$ do not have to be single values but can be ranges of thickness, in which case the average of the granular spectral values is taken. Use of area opening[15] instead of opening to produce granular spectrum may be beneficial.

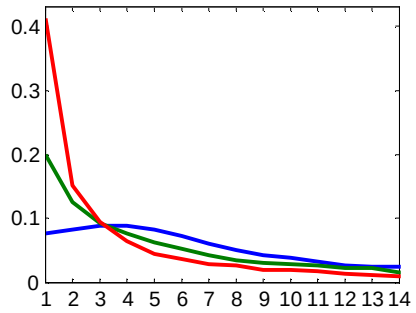

Fig. 26. Granular spectrum for negative (blue), intermediate (green) and positive (red) states of Transfluor assay. X:size of opening, Y:fraction of the image volume at this opening.

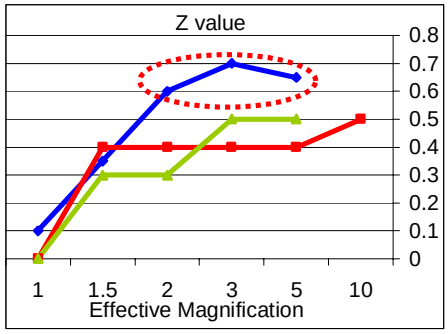

Fig. 27. Dependency of z-value for relative granularity on magnification and image size. Blue – image size 0.4mm^2, green and red – image size 0.1mm^2. The range of best assay performance is outlined.

To study the effects of the magnification and image sizes on relative granularity we used z-values because a detailed dose curve was not available. Two sets of images were used for experiments: one set for the positive state and one for the negative state. In each set one image was acquired using a 10X objective and one using a 20X objective, both with 2 by 2 binning; so in terms of spatial resolution we refer to them here as 5X and 10X magnifications. This has the benefit of making the plots comparable with other assays described. The image at 20X corresponds to the middle quarter of the 10X image. In addition we used an image that is the middle quarter of the 10X image. Each of the three images was divided in four fragments and the assay measure – relative granularity - was calculated for each of the fragments for the negative and positive state. Z values were then calculated using positive and negative sets. Fig. 27 shows the window of good assay performance at magnifications of 2X and above and image size of 0.4mm^2. The algorithm presented above has several desirable features – it requires no segmentation, scales well with magnification, has clear biological meaning, does not require any user parameters and is not sensitive to overall image intensity, which can be caused by differences in camera setting.

In the previous sections we have demonstrated two different assays and two very different methods of image analysis. In both cases the results show that the assays can be miniaturized in terms of required magnification and image size to be practical on CellCards.

8. CONCLUSION

The desire for increased information on compounds early in the drug discovery program has dramatically increased the use of cell based assays instead of, or in addition to, standard biochemical assays. We have developed a new platform that allows the simultaneous analysis of multiple cell lines in one well, thus providing single-well profiling of compounds. This platform is based on a new non-positional array technology tailored to cells. The platform is enabled by new imaging algorithms to identify and analyze cell-based data.

REFERENCES

1. Nolan, J.P. & Mandy, F.F. “Suspension array technology: new tools for gene and protein analysis”, *Cell Mol Biol* **47**, 1241-1256, 2001.
2. Zhou, H., Roy, S., Schulman, H. & Natan, M.J. “Solution and chip arrays in protein profiling”, *Trends Biotechnol* **19**, S34-39, 2001.
3. Iannone, M.A. et al. “Multiplexed molecular interactions of nuclear receptors using fluorescent microspheres”, *Cytometry* **44**, 326-337, 2001.
4. Armstrong, B., Stewart, M. & Mazumder, A. “Suspension arrays for high throughput, multiplexed single nucleotide polymorphism genotyping” *Cytometry* **40**, 102-108, 2000.
5. Martins, T.B. “Development of internal controls for the Luminex instrument as part of a multiplex seven-analyte viral respiratory antibody profile”, *Clin Diagn Lab Immunol* **9**, 41-45, 2002.
6. O. Beske, J. Guo, J. Li, D. Bassoni, K. Bland, H. Marciniak, M. Zarowitz, V. Temov, I. Ravkin, S. Goldbard "A novel encoded particle technology that enables simultaneous interrogation of multiple cell types", *J. Biomol. Screening*, 2004 (in press).
7. J.-H. Zhang, T.D.Y. Chung, K.R. Oldenburg “A simple statistical parameter for use in evaluation and validation of high throughput screening assays”, *J. Biomol. Screening* ***4***: pp. 67-73, 1999
8. I. Ravkin, V. Temov, "Automated microscopy system for detection and genetic characterization of fetal nucleated red blood cells on slides", *Proceedings of SPIE* (Optical Investigation of Cells In Vitro and In Vivo), v. 3260, pp. 180-191, 1998.
9. J. Serra, *Image Analysis and Mathematical Morphology*, Vol. 1. Academic Press, London, 1989
10. S. Beucher and F. Meyer, “The Morphological Approach to Segmentation: The Watershed Transformation” in: *Mathematical Morphology in Image Processing*, E.R. Dougherty – Ed., pp. 433 – 481, Marcel Dekker, New York, 1993
11. L. Vincent, P. Soille, "Watersheds in Digital Spaces: An Efficient Algorithm Based on Immersion Simulations", *IEEE Transactions of Pattern Analysis and Machine Intelligence*, **13**, No. 6, pp. 583-598, 1991
12. N. Otsu "A Threshold Selection Method from Gray-Level Histograms," *IEEE Transactions on Systems, Man, and Cybernetics*, ***9***, No. 1, pp. 62-66, 1979
13. Maragos, P. “Pattern spectrum and multiscale shape representation”, *IEEE Transactions on Pattern Analysis and Machine Intelligence*, **11**, N 7, pp. 701-716, 1989
14. L. Vincent "Granulometries and Opening Trees", *Fundamenta Informaticae*, **41**, No. 1-2, pp. 57-90, IOS Press, 2000.
15. L. Vincent "Morphological Area Opening and Closing for Grayscale Images", Proc. NATO Shape in Picture Workshop, Driebergen, The Netherlands, pp. 197-208, 1992.
16. I. Ravkin, V. Temov “Bit representation techniques and image processing”, Applied Informatics, v.14, pp. 41-90, Finances and Statistics, Moskow, 1988 (in Russian)
17. “System for cell-based screening”, US patent 5989835.
18. “System and method for automatic color segmentation and minimum significant response for measurement of fractional localized intensity of cellular compartments”, International patent application WO03078965
19. “Methods for determining the organization of a cellular component of interest", US patent application 20030059093.
20. “Ray-based image analysis for biological specimens”, US patent application 20030202689.
21. I. Ravkin, et al. "Multiplexed cell analysis on CellCards for drug discovery", *Proceedings of SPIE* (Microarrays, Combinatorial Techniques and High Throughput Screening) Vol. 5328, 2004 (in press)